

Discovery of Extensive Optical Emission Associated with the X-ray Bright, Radio Faint Galactic SNR G156.2+5.7

Christopher L. Gerardy¹ & Robert A. Fesen²

¹*Astrophysics Group, Imperial College London, Blackett Laboratory, Prince Consort Road, London SW7 2AZ, UK*

²*Department of Physics & Astronomy, Dartmouth College, 6127 Wilder Laboratory, Hanover, NH 03755-3528, USA*

13 Aug 2006

ABSTRACT

We present wide-field $H\alpha$ images of the Galactic supernova remnant G156.2+5.7 which reveal the presence of considerable faint $H\alpha$ line emission coincident with the remnant's X-ray emission. We also present low-resolution optical spectra for a few representative emission regions. The outermost $H\alpha$ emission consists largely of long and thin (unresolved), smoothly curved filaments of Balmer-dominated emission presumably associated with the remnant's forward shock front. Patches of brighter $H\alpha$ emission along the western, south-central, and northeastern regions appear to be radiative shocked ISM filaments like those commonly seen in supernova remnants, with relatively strong [O I] $\lambda\lambda 6300, 6364$ and [S II] $\lambda\lambda 6716, 6731$ line emissions. Measured [S II] $\lambda\lambda 6716, 6731/H\alpha$ ratios range from 0.84 to 1.57.

Comparison of the observed $H\alpha$ emission with the *ROSAT* PSPC X-ray image of G156.2+5.7 shows that the thin Balmer-dominated filaments lie along the outermost edge of the remnant's detected X-ray emission. Brighter radiative emission features are not coincident with the remnant's brightest X-ray or radio regions. Areas of sharply weaker X-ray flux seen in the *ROSAT* image of G156.2+5.7 appear spatially coincident with dense interstellar clouds visible on optical and *IRAS* 60 and 100 μm emission images, as well as maps of increased optical extinction. This suggests significant X-ray absorption in these regions due to foreground interstellar dust, especially along the western and southern limbs. The close projected proximity and alignment of the remnant's brighter, radiative filaments with several of these interstellar clouds and dust lanes hint at a possible physical interaction between the G156.2+5.7 remnant and these interstellar clouds and may indicate a smaller distance to the remnant than previously estimated.

Key words: ISM: individual (G156.2+5.7) – supernova remnants

1 INTRODUCTION

A majority of the ~ 230 currently confirmed Galactic supernova remnants (SNRs) listed in the latest SNR catalogue (Green 2004) were first identified through radio surveys. However, with the advent of sensitive X-ray satellites, about half a dozen remnants have now been discovered via their X-ray emission (cf. Busser, Egger, & Aschenbach 1996 and references therein).

The first Galactic SNR discovered through its X-ray emission was reported by Pfeffermann, Aschenbach, & Predehl (1991). They found a previously unknown Galactic SNR based on the *ROSAT* detection of a relatively bright and nearly circular 108' diameter emission structure centred on $\alpha(\text{J2000}) = 4^{\text{h}} 59^{\text{m}} 7^{\text{s}}$, $\delta(\text{J2000}) = 51^{\circ} 46' 35''$. With an estimated 0.1 – 2.4 keV

X-ray flux of 1.9×10^{-10} erg cm^{-2} s^{-1} , this new remnant ranked among the ten brightest X-ray Galactic SNRs known at that time. Pfeffermann et al. (1991) concluded that the remnant was located in a region of very low interstellar density (0.01 atoms cm^{-3}), which might help account, in part, for the remnant's lack of strong radio emission.

The new remnant, designated G156.2+5.7 (also RXJ04591+5147), was subsequently detected and confirmed in the radio by Reich, Fuerst, & Arnal (1992). In contrast to the object's bright X-ray flux, its 1 GHz radio surface brightness of 5.8×10^{-23} W m^{-2} Hz^{-1} sr^{-1} ranks it as perhaps the faintest Galactic SNR currently known (Green 2004), being a factor of two in 1 GHz surface brightness below that of the exceptionally radio faint but optically [O III] bright remnant, G65.3+5.7 (Gull, Kirshner & Parker 1977; Reich et al. 1979). Follow-up searches for a central radio

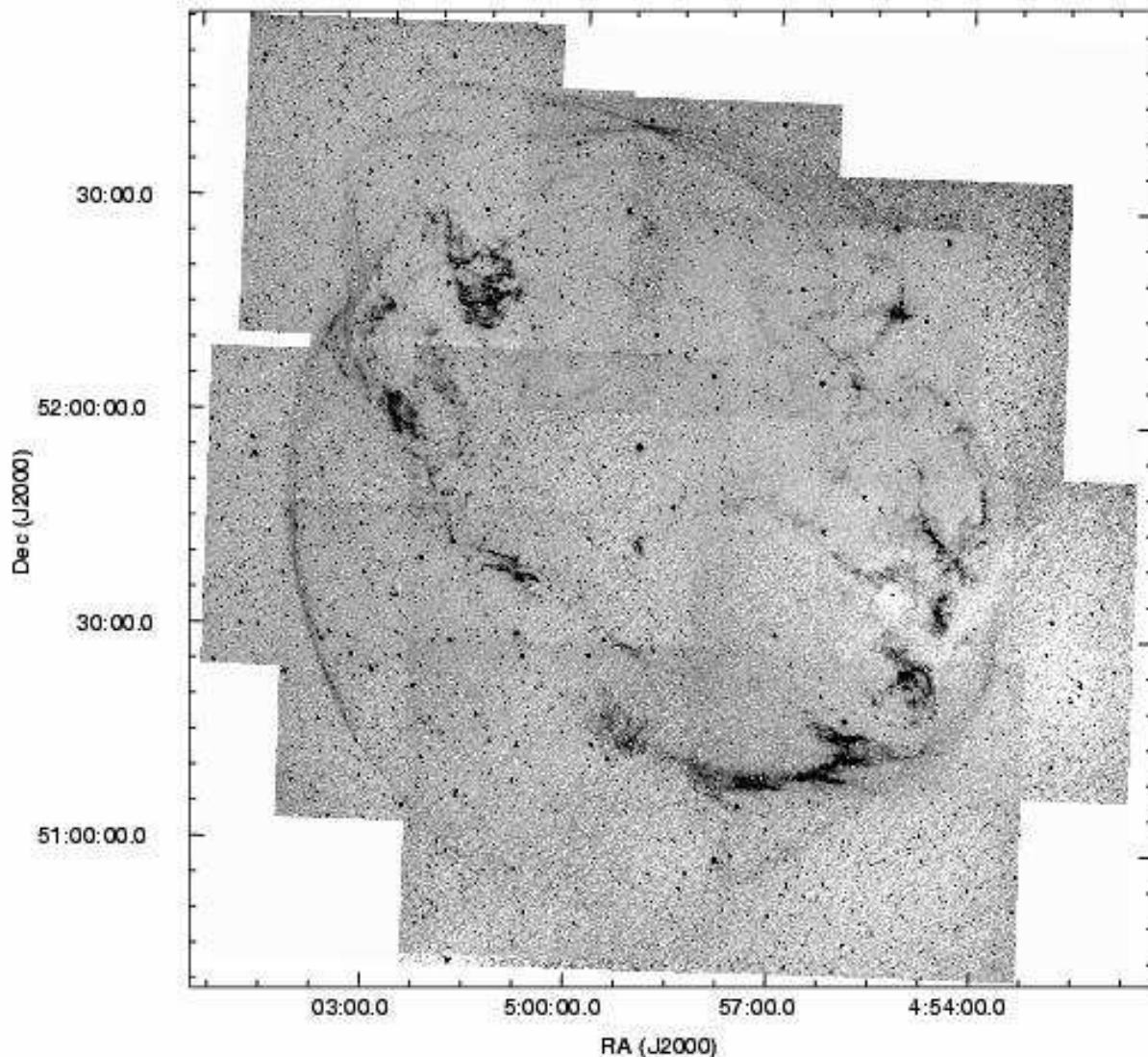


Figure 1. $H\alpha$ mosaic image of the G156.2+5.7 supernova remnant. Two distinct emission morphologies are seen: a faint rim of thin filamentary emission which runs most of the way around the remnant; and patches of much brighter emission with a clumpy, complicated structure. Note the white dust absorption patch along the remnant’s western limb. To reduce the appearance of background noise the data have been smoothed slightly using a Gaussian filter.

pulsar or central compact object have proven unsuccessful (Lorimer et al. 1998; Kaplan et al. 2006).

Since shortly after its discovery, G156.2+5.7 has been studied only in the X-rays. Using the *ASCA* satellite, Yamauchi et al. (1999, 2000) found both hard and soft X-ray components, an estimated Sedov age of $\sim 1.5 \times 10^4$ yr, and an ambient gas density of $\sim 0.2 \text{ cm}^{-3}$. More recently, Pannuti & Allen (2004) used both *ASCA* and *RXTE* to study the the northwestern rim of G156.2+5.7 and investigate the presence of a non-thermal X-ray component and cosmic-ray acceleration.

Pfeffermann et al. (1991) reported finding no associated optical emission on the Palomar Sky Survey plates and there are no discernible emission features in this region visible on the relatively deep, narrow passband filter images of Parker, Gull, & Kirshner (1979) in their emission-line survey of the Milky Way. However, here we present wide field

$H\alpha$ images of the remnant which reveal a remarkably extensive and complex optical emission structure covering a large fraction of the remnant’s X-ray shell.

2 OBSERVATIONS

2.1 Narrow-band $H\alpha$ Imaging

Wide-field imaging of G156.2+5.7 (hereafter referred to as G156) was performed using the McDonald Observatory 0.76-m telescope and the Prime-Focus Corrector (PFC) camera (Claver 1992). This system uses a 2048×2048 Loral Fairchild front-side illuminated CCD which produces a plate scale of $1''.35$ per pixel and an unvignetted field of view of $46'.1 \times 46'.1$ with little spatial distortion ($< 0''.5$, far better than the typical seeing).

Narrow passband imaging was carried out using a pair

of matched interference filters (FWHM 30 Å) centred at 656.8 nm (= H α) and 651.0 nm (= adjacent red continuum). These filters were optimised for an f/7 setup, which caused some concern given the faster (f/3) optics of the 0.76-m/PFC setup. However, tests on-sky suggest that the faster optics did not dramatically affect the performance. In particular we detect no significant change in H α sensitivity between the centre and the edge of the detector (other than the variation due to the flat-field). The H α setup suffers from a strong internal reflection which is not present in the continuum images, and results in a characteristic halo around bright point sources.

Dome flats for both filters were obtained nightly and, whenever clear, twilight flats were also obtained in morning and evening twilight. Since the S/N of the dome flats was significantly better, they were the primary images used for flat-field correction. However, the twilight flats were used to perform illumination corrections on the nightly dome flats. The illumination image was created via a two-stage process. First, all the twilight flats were combined, and each individual twilight flat was divided by the resulting average twilight image. Any twilight frames which showed a significant gradient or other structure relative to the average were then removed and a second image was created using the reduced set of twilight frames. Each of the nightly dome flats was then divided by this refined twilight image, and the illumination correction for the dome flat created via a 2-D, low-order polynomial fit.

Observations of G156 were carried out over three nights, 12, 18, & 19 January 2004, in conditions ranging from photometric to moderate cirrus. Since the remnant is much larger than the PFC field of view, it was covered in 13 partially overlapping telescope pointings. For each pointing a pair of 1000 s exposures was obtained in both the H α and 6510 continuum filters. As the PFC does not have a working guider, the images were unguided, and the tracking rate of the telescope manually adjusted using an empirical mapping of the tracking rate for different declinations and hour angles. Inevitably, this open-loop tracking and the long exposures required for narrow-band imaging resulted in some images with relatively poor point-spread functions (PSFs). At the scale of the remnant, this degradation of the image quality is not a serious problem. However, the PSF of the paired H α and continuum images are not always a perfect match if the tracking drift was larger in one of the two images. Even in well tracked image pairs, the internal reflections in the H α filter leave a residual halo around bright stars in the continuum subtracted images.

After bias and flat-field correction, each pair of H α and continuum images were registered via cross correlation routines in IRAF, and trimmed to the overlapping region. The H α images obtained in non-photometric data were scaled to match the flux levels in the photometric frames by matching the flux in aperture photometry of stars in the overlapping regions between the different pointings. For a couple of fields, there were no adjacent pointings taken in photometric conditions, and the flux was set matching re-scaled H α flux in an adjacent image. The relative flux across the entire remnant is probably accurate to $\sim 20\%$.

After setting the flux levels for each H α image, the paired continuum image was scaled to match using aperture photometry of a large number of field stars. The con-

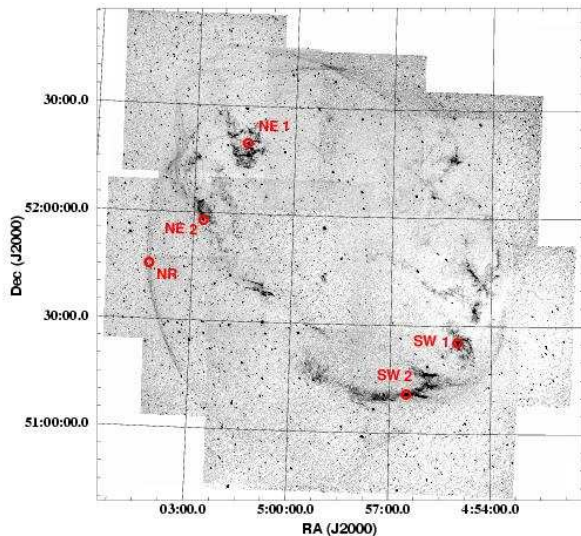


Figure 2. H α image of the G156 SNR with the locations of the observed optical spectra shown.

tinuum image was then subtracted from the H α image at each pointing, and the resulting continuum subtracted image was combined into a single mosaic. The continuum subtraction process often left a small residual level in the background, which was removed before the images were mosaiced together. This reduced the ‘patchwork quilt’ appearance of the final mosaic, although variations in signal-to-noise and small flat-fielding errors mean that the combination of these multiple pointings is not seamless (see Fig. 1). The reduced 6510 Å images were also similarly combined to create a mosaic continuum image.

2.2 Optical Spectroscopy

Low-dispersion optical spectra of a few of the remnant’s brighter emission knots were obtained on three nights between 10 – 12 September 2004 using the MDM 2.4-m telescope at Kitt Peak Arizona and the Modular Spectrograph with a 600 lines mm $^{-1}$ 6000 Å blaze grating and a 1’5 \times 4’ slit. Spectra were taken at four locations in the remnant’s detected optical emission, two in the NE and SW (see Fig. 2) with the slit orientated north-south across relatively bright features of the detected optical emission.

Total exposure times ranged from 300 to 900 s yielding spectra with an effective coverage of 6000 – 8000 Å and a spectral resolution of $\simeq 2$ Å. Standard IRAF software was used for the data reduction with wavelength calibration using Hg, Ne, and Xe lamps and flux calibration via Massey & Gronwall (1990) standard stars. Although all three nights were photometric, seeing varied between 1’0 – 1’5. As a result, slit light losses were considerable at times due to the variable seeing conditions and guiding errors. Consequently, our measured absolute flux values are only accurate to $\pm 25\%$.

A separate 2000 s spectrum was taken of the suspected Balmer-dominated, non-radiative filament along the remnant’s eastern limb. These data were obtained on 9 October 2005 under non-photometric conditions using the MK III

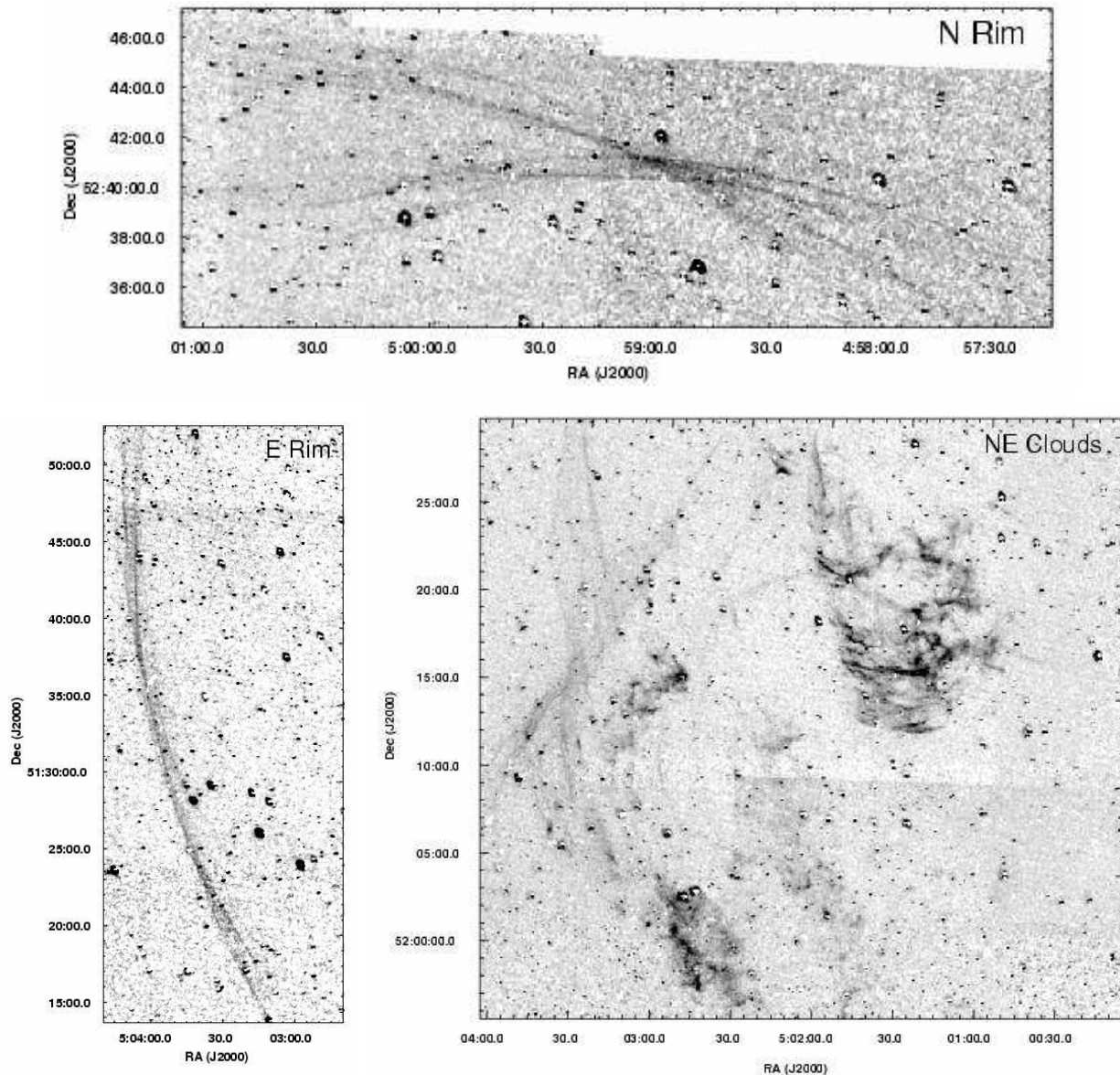


Figure 3. Enlargements of the $H\alpha$ mosaic image showing thin, overlapping filamentary arcs near the middle of the northern rim (top), and eastern rim (left) of G156. These filaments are likely non-radiative shocks producing Balmer-dominated emission. A mixture of thin non-radiative features and brighter emission filaments can be seen near the northeast corner of the remnant (right). To reduce the appearance of background noise the data have been smoothed using a Gaussian filter.

spectrograph on the MDM 2.4-m telescope. A $1''.7 \times 4'$ east-west aligned slit together with a $300 \text{ lines mm}^{-1}$ 5000 Å blaze grism was used to yield a spectrum coverage of 5500 – 8000 Å, calibrated as before with Hg, Ne, and Xe lamps and Massey & Gronwall (1990) standard stars.

3 RESULTS

3.1 $H\alpha$ Mosaic Image

Our continuum subtracted $H\alpha$ mosaic image is shown in Figure 1. The mosaic shows an extensive and complex $H\alpha$ emission structure. While numerous features are readily apparent in this image, they are actually quite faint, with an es-

timated surface brightness of $\leq 2 \times 10^{-16} \text{ erg cm}^{-2} \text{ arcsec}^{-2}$ for most of the brighter regions. The optical emission seen here is invisible on the Palomar Sky Survey, in the relatively deep narrow passband filter images of Parker et al. (1979), and is not listed in the Atlas of Galactic Nebulae (Neckel & Vehrenberg 1985).

Two distinct morphologies are seen; faint, thin (often unresolved) filamentary arcs some tens of arc minutes long, and much brighter more diffuse filamentary features like those seen in many optical Galactic SNRs. The thin filaments are primarily found near the edges of the detected optical emission structure, and are brightest along the eastern limb ($\alpha = 5^{\text{h}}03^{\text{m}} - 5^{\text{h}}04^{\text{m}}$, $\delta = 51^{\circ}15' - 51^{\circ}50'$) and the

northern limb ($\alpha = 4^{\text{h}}58^{\text{m}} - 5^{\text{h}}01^{\text{m}}$, $\delta = 52^{\circ}40'$) of the G156 SNR.

Two regions exhibiting thin and partially overlapping filamentary arcs are shown in greater detail in the upper and lower left panels of Figure 3. The morphology of such filamentary emission is reminiscent of the non-radiative, Balmer-dominated shock emission along the outer edges of supernova remnants (e.g., the Cygnus Loop, Tycho’s SNR, and SN 1006). Indeed, a spectrum of these filaments along the east rim of the detected emission structure (at the point labelled “NR” in Figure 2) showed only $\text{H}\alpha$ line emission within the 6000 – 8000 Å wavelength range. Such a spectrum is consistent with it being a Balmer filament associated with non-radiative shock emission. Although brightest to the north and east, these filaments can be seen to form a nearly unbroken shell of emission surrounding the brighter, more diffuse emission regions. These thin filaments fade out in the northwest near $\alpha = 04^{\text{h}}55^{\text{m}}$, $\delta = 52^{\circ}15'$ and in the south at $\alpha = 5^{\text{h}}00^{\text{m}}$, $\delta = 50^{\circ}55'$.

The lower right panel of Figure 3 shows examples of both the faint filamentary emission and much brighter, more diffuse and clumpy filament type emission. Clumpy filaments are the brightest $\text{H}\alpha$ features detected in the G156 region and form a patchy arc which loops from the NE down to the SW region of the remnant region (see Fig. 1). In the NE, this arc is dominated by a large complex of filaments at $\alpha = 5^{\text{h}}01^{\text{m}} - 5^{\text{h}}02^{\text{m}}$, $\delta = 52^{\circ}10' - 52^{\circ}25'$, which exhibits considerable internal structure. We will refer to this feature as the “NE filament complex”. In the southwest portion of the $\text{H}\alpha$ mosaic image, this clumpy type of emission forms a bright ridge which is broken by an apparent foreground dust-lane near $\alpha = 4^{\text{h}}54^{\text{m}} - 4^{\text{h}}55^{\text{m}}$, $\delta = 51^{\circ}25' - 51^{\circ}45'$. Small patches of clumpy emission are also seen in the NW near the break in the outer thin filamentary emission, and near the centre of the image.

3.2 Comparison of Detected $\text{H}\alpha$ Emission with X-ray and Radio Emission

Comparison of the observed $\text{H}\alpha$ emission with a *ROSAT* PSPC 2° Survey X-ray image of G156 suggests that virtually all of the detected optical emission is associated with the G156 remnant. Figure 4 shows the *ROSAT* PSPC X-ray image (0.1 – 2.4 keV) in red with our $\text{H}\alpha$ emission mosaic superimposed in green.

This figure shows that the detected gentle arcs of thin filamentary emission lie along the outermost edge of the remnant’s observed X-ray emission, confirming that these are indeed non-radiative emission from the outer blast wave of the supernova remnant. Along the NE limb, the non-radiative filaments bulge outward a bit from their otherwise relatively circular arc. This bulge in the optical corresponds well to faint extended X-ray emission seen in the *ROSAT* image. The rim of $\text{H}\alpha$ emission fades out close to the region in the southeast where the X-ray emission is also faint. In contrast, the clumpy optical emission is less clearly associated with emission structures in the X-ray image, but appears to lie somewhat near the boundaries of darker (X-ray faint) regions in the *ROSAT* image.

As a follow-up to our detection of $\text{H}\alpha$ in this region, we conducted an on-line search of survey data of the G156 re-

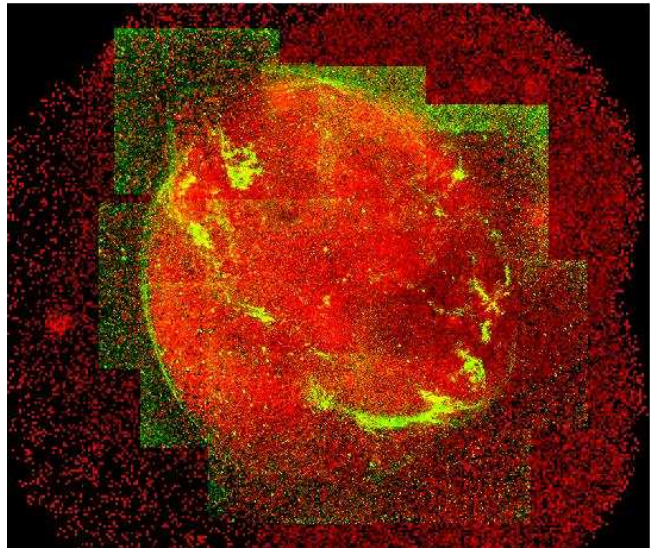


Figure 4. The X-ray image (red) of G156 from the *ROSAT* PSPC 2° Survey overlaid with our continuum subtracted $\text{H}\alpha$ image (green). The X-ray and $\text{H}\alpha$ images are displayed using a square-root and log intensity scales, respectively. The non-radiative $\text{H}\alpha$ filaments lie just beyond the outer edge of the X-ray emission. A weak bulge of X-ray emission in the NE is similarly bounded by faint $\text{H}\alpha$ filaments extending outward from the otherwise quite circular boundary of G156.

gion with the *Skyview Virtual Observatory*¹ (McGlynn et al. 1996). Surprisingly, the $\text{H}\alpha$ emission we found associated with G156 was, in fact, well detected (but unreported) by the Virginia Tech Spectral Line Survey (VTSS) (Finkbeiner 2003, Fig. 5, upper left), albeit at much lower spatial resolution. Comparison of our $\text{H}\alpha$ mosaic with the VTSS image shows good agreement between the two data sets after allowing for the much lower spatial resolution of the VTSS image.

Small portions of the G156 remnant can also be weakly seen in the 325 MHz Westerbork Northern Sky Survey (WENSS Rengelink et al. 1997, Fig. 5, lower left), showing a similar radio structure to that seen at 1448 and 2695 MHz (Reich et al. 1992). The remnant’s radio emission appears nearly anti-correlated with the optical Balmer filaments, as it shows only two faint filaments to the south where the Balmer-dominated rim emission is weakest, and to the northwest where non-radiative filaments are poorly detected (although there is faint diffuse $\text{H}\alpha$ emission and a bright clump of diffuse emission here.) The VTSS $\text{H}\alpha$, *ROSAT* X-ray, and WENSS 325 MHz images are all shown in Figure 5 – in the upper left, upper right and lower left, respectively – with all three overlaid as a three-colour image in the lower right.

3.3 Optical Spectra of G156 Filaments

The optical spectra of four filaments of G156’s brighter emission labeled in Figure 2 are shown in Figure 6. Observed line fluxes and ratios from these data are listed in Table 1. The individual emission line profiles for $\text{H}\alpha$ and [S II] were

¹ <http://skyview.gsfc.nasa.gov>

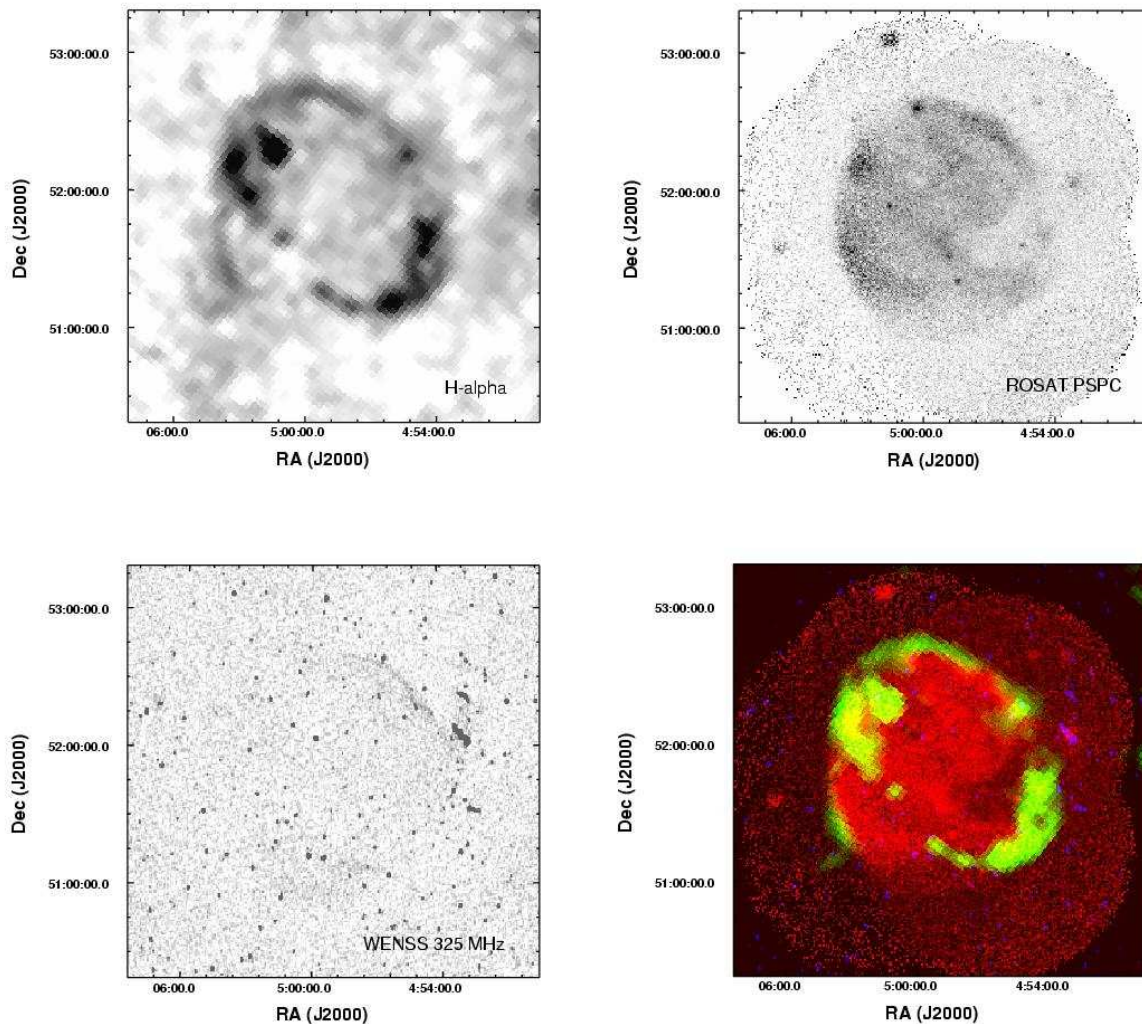


Figure 5. Upper left: Low spatial resolution $H\alpha$ image of G156 from the Virginia Tech Spectral Line Survey (VTSS; Finkbeiner 2003). Upper Right: X-ray (0.1 – 2.4 keV) image of G156 from the *ROSAT* PSPC 2° Survey. Lower Left: 325 MHz image of G156 from the Westerbork Northern Sky Survey (WENSS; Rengelink et al. 1997). Lower Right: Colour-composite of these three images with X-rays in red, $H\alpha$ in green, and 325 MHz in blue.

unresolved at a spectral resolution of 2 \AA , with no radial velocities observed above 150 km s^{-1} .

The well established criteria for identifying shock emission is a $[\text{S II}]/H\alpha$ ratio greater than 0.4 (Raymond 1979; Fesen, Blair, & Kirshner 1985; Blair & Long 1997). All four G156 spectra exhibit much larger $[\text{S II}]/H\alpha$ ratios than this threshold (0.8 – 1.6; see Table 1), strongly indicating that the detected emission filaments are shocked interstellar gas. Likewise, the relatively strong $[\text{O I}] \lambda\lambda 6300, 6364$ emission seen in these spectra also in line with shock emission, since $[\text{O I}]$ line emission is quite weak relative to $H\alpha$ in H II regions and photoionized nebulae (Fesen, Blair, & Kirshner 1985).

Overall, the observed spectra are typical of radiative emission in supernova remnants, even down to the presence of $[\text{Ar III}] \lambda 7135$, $[\text{Fe II}] \lambda 7155$, and $[\text{Ca II}] \lambda 7291$ seen in the spectrum of SW1. In summary, both the morphology of the brighter emission nebulae seen in the G156 region and the observed spectra of these nebulae suggest that these

emissions constitute radiative shocked material associated with the G156 supernova remnant.

Electron densities, N_e , for each spectrum were calculated using the measured $\lambda 6716/\lambda 6731$ $[\text{S II}]$ ratio values and the Space Telescope Science Data Analysis System task “nebular.temden” which is based on a five-level atom approximation and assuming $T = 10^4 \text{ K}$. The observed $[\text{S II}] 6716/6731 \text{ \AA}$ line ratios imply moderately high post-shock densities $N_e = 200 - 300 \text{ cm}^{-3}$. Such densities imply a much higher ambient density than the estimates from analysis of the X-ray emission $n_0 = 0.01 - 0.2 \text{ cm}^{-3}$ (Pfeffermann et al. 1991; Yamauchi et al. 1999, 2000). Assuming a shock velocity $\sim 100 \text{ km s}^{-1}$, a $[\text{S II}]$ derived electron density of 300 cm^{-3} suggests a preshock density of around 10 cm^{-3} (Fesen & Kirshner 1980). The obvious suggestion is that G156 is interacting with a clumpy interstellar medium resulting in patches of radiative emission where the blast wave

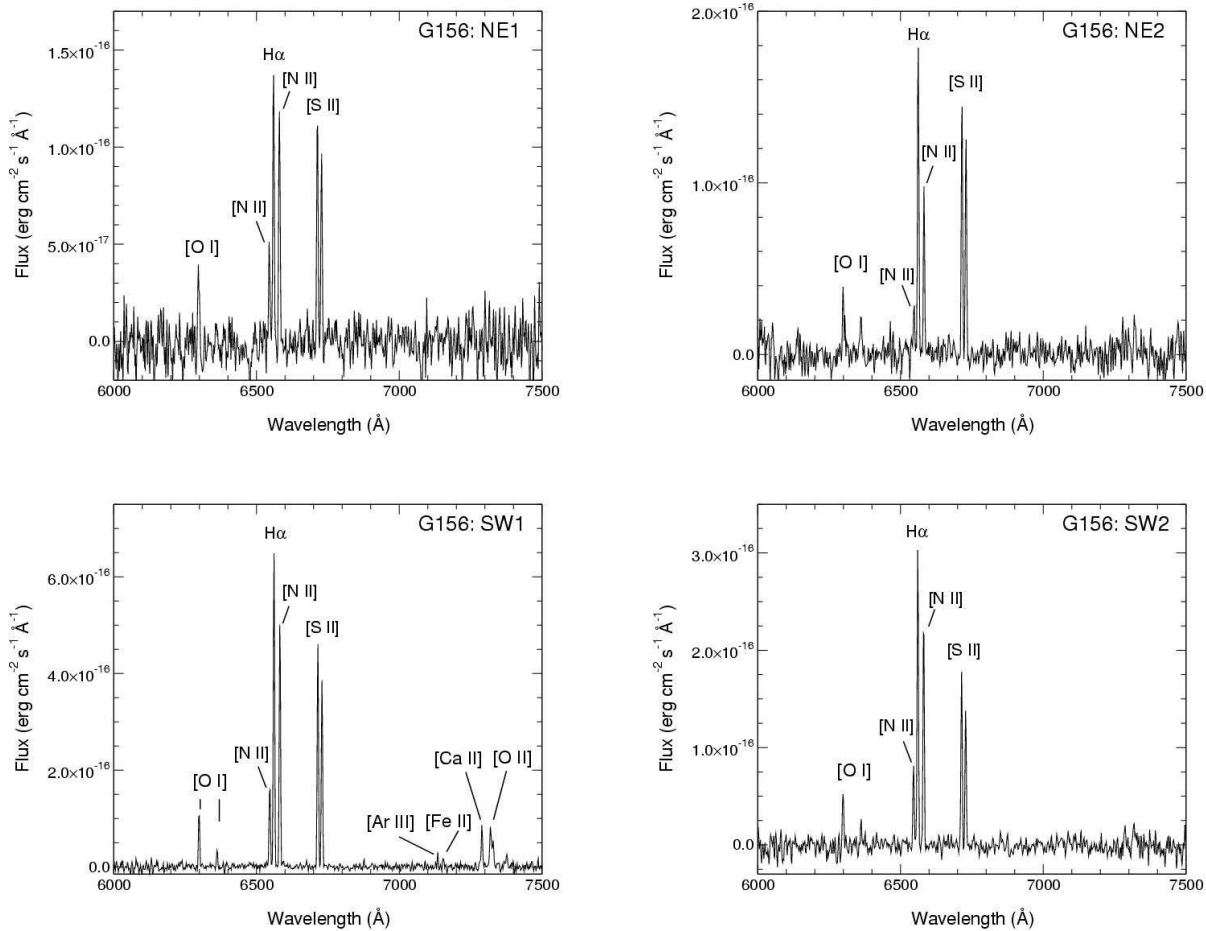


Figure 6. Optical spectra of emission from radiative shocks at four locations in G156. The locations are labelled in Figure 2.

is running into dense clouds, and showing only a Balmer-dominated rim of emission in much lower-density regions.

3.4 ISM Clouds in the G156 Region

There appear to be several dense interstellar clouds along the line of sight to G156. Figure 7 is a composite image showing both the 6510 Å continuum mosaic (greyscale) and the continuum-subtracted H α (red) mosaic for a section in the northeastern portion of the remnant. The bright H α emission near the left of the image was referred to earlier as the “NE filament complex”. The lower part of this emission complex appears about 10′ – 20′ NE of a dark interstellar cloud which appears in the 6510 Å image as a region lacking in background stars but with a faint continuum emission, presumably due to ambient radiation scattered by dust near the surface of the cloud. Very weak continuum emission is detected extending from the upper NE end of the cloud which appears to end at approximately the southern extent of the NE filament complex’s H α emission. The larger opaque cloud visible just below the centre of this image is a known Bok globule (α [J2000] = 4^h59^m50.74^s, δ [J2000] = 52°04′43.8″; LDN 1439; CB 26; Clemens & Barvainis 1988; Clemens, Yun, & Heyer 1991) and harbors a young stellar object (YSO) with an associated Herbig-Haro object located

some 6.15′ off to the northwest (HHO 494; Stecklum et al. 2004).

The projected spatial coincidence between shocked radiative emission in the NE filament complex and this dusty interstellar cloud makes it tempting to suggest that part of the remnant is actually colliding with the outskirts of this cloud. The bright H α emission to the SW appears similarly spatially coincident with a large region of high extinction which results in the dark dust lane seen in Figure 1. However, there is no clear evidence in the optical images for significant dust obscuration near some of the other radiative emission features.

However, there is clear evidence that much of the structure in the *ROSAT* image is due to X-ray absorption from these interstellar dust clouds. The dark clouds near the NE filament complex and along the southwest rim of G156 are exactly coincident with dark patches seen in the X-ray image. In Figures 4 and 5, the NE radiative filament complex appears as a bright green feature near the NE rim of the remnant, with the dark interstellar cloud to its southwest visible as a virtual ‘hole’ in the X-ray emission. Similarly, along the southwest edge of the remnant, a large patch of significantly decreased X-ray emission can be seen in the *ROSAT* X-ray image coincident with a large dust lane visible in the H α mosaic image (Fig. 1). This western patch of



Figure 7. A composite image showing both the continuum 6510 Å image (greyscale) and the continuum subtracted H α image (red) for the region near the “NE filament complex”. The bright clump of H α emission appears near a large dark cloud which is seen in the image as both faint continuum emission and a lack of background stars. The gap between the southern end of the H α emission and the northeastern end of the dark cloud also shows faint continuum emission. This apparent spatial coincidence is perhaps suggestive of a cloud-supernova remnant interaction.

Table 1. Observed Relative Line Intensities

Line	ID	NE1	NE2	SW1	SW2
6300	[O I]	88	62	50	45
6548	[N II]	108	40	80	85
6563	H α	300	300	300	300
6583	[N II]	270	145	233	245
6716	[S II]	225	250	213	135
6731	[S II]	180	220	180	115
7135	[Ar III]	10	...
7155	[Fe II]	9	...
7291	[Ca II]	36	20
7319,30	[O II]	54	30
6716/6731	[S II] ratio	1.25	1.14	1.18	1.16
6716,31/6563	[S II]/H α	1.35	1.57	1.31	0.84
6300,63/6563	[O I]/H α	0.40	0.27	0.22	0.20
	H α Flux ^a	8.9	10	36	30
	N _e ^a	175	325	270	300

^a H α flux is listed in units of 10^{-16} erg cm $^{-2}$ s $^{-1}$.

^b Electron densities are given in units of cm $^{-3}$.

faint X-ray emission extends well into the interior of the remnant and is coincident with a region showing several dusty interstellar clouds. One of these dusty clouds (dia. = 5′) is associated with the young T-Tauri star V347 Aur (α [J2000] = 4^h56^m56.7^s, δ [J2000] = 51°30′56″; RNO 33; Cohen 1978, 1980; Osterloh & Beckwith 1995 in LDN 1438 (Lynds 1962) at an estimated distance of around 250 – 300 pc.

The coincidence between the dark ISM clouds and the X-ray emission ‘holes’ can be clearly seen in Figures 8 and 9. In Figure 8, we compare the *ROSAT* X-ray image (red) with the *IRAS* 60 μ m image (green). The dark clouds ap-

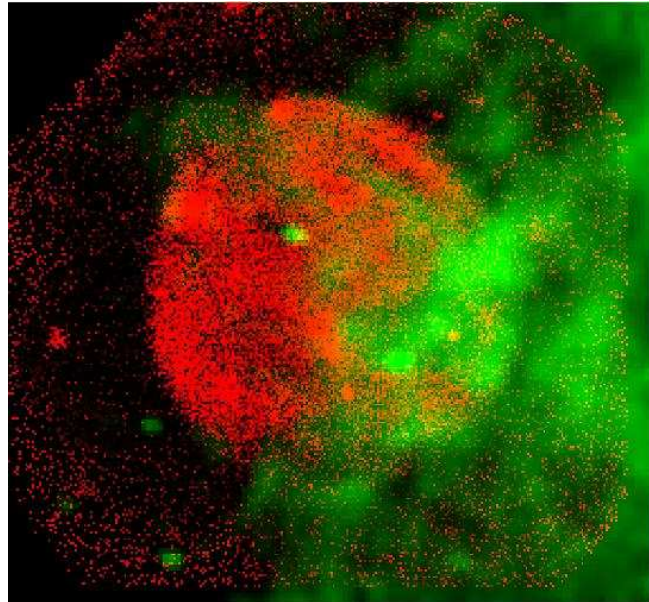


Figure 8. X-ray image (red) of G156 from the *ROSAT* PSPC 2° Survey overlaid with the *IRAS* 60 micron image (green) for the same region. Both images are displayed using a square-root intensity scale. This shows the excellent correlation between the warm ISM cloud regions and several major features seen in the X-ray image due to foreground dust absorption. The bright *IRAS* point source in the SW quadrant of G156 is coincident with the T-Tauri star V347 Aur.

pear in emission in the *IRAS* image and correlate very well with both the cloud near the NE filament complex, and the large triangular shaped emission hole along the western portion of the remnant. Furthermore, there appears to be *IRAS* emission associated with other X-ray faint regions of G156,

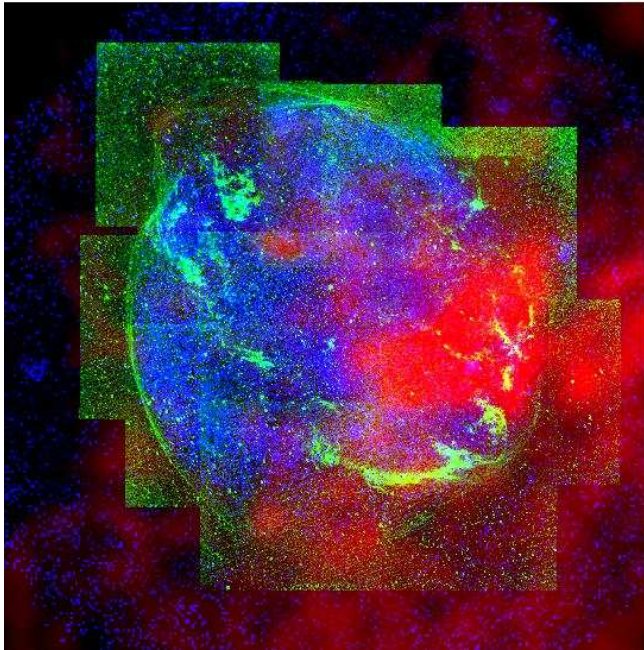


Figure 9. X-ray image (blue) of G156 from the *ROSAT* PSPC 2° Survey overlaid with our H α mosaic (green) and the 6' resolution A_V extinction map (red) of Dobashi et al. (2005). The Both the X-ray and H α images are displayed using a square-root intensity scale. The A_V map is shown on a log scale and peaks around $A_V = 3$. This image shows the excellent correlation between the foreground dust clouds and major features seen in the X-ray image.

including its southern limb, a region near the X-ray/optical bulge in the NE, and a NE–SW oriented stripe near the NW edge of the remnant. However, in a few spots, some 60 μm emission also appears to be associated with optical emission from G156. In particular, a faint ring of emission (difficult to see in Figure 8) appears to correlate with the H α Balmer filaments, and the NE X-ray emission bulge can also be seen as an emission feature in the 60 μm image.

Such confusion between interstellar dust and SNR emission is not present in Figure 9, which shows the *ROSAT* X-ray image (blue) the H α mosaic (green) and the 6' resolution A_V extinction map (red) of Dobashi et al. (2005). Since this A_V map is based solely on a star count analysis of data from the Digitized Sky Survey, there can be no confusion with line emission features. However, once again the interstellar cloud near the NE filament complex and the large triangular region in the SW are seen coincident with high extinction zones in the A_V map, as are the absorbing regions along the remnant's southern limb and the NE–SW stripe along the northern limb.

The observed coincidences between X-ray emission holes and dusty interstellar clouds strongly indicate that the clouds lie in front of the remnant creating X-ray absorption shadows on the resulting X-ray image of the G156 remnant. In fact, many of the structures seen in the *ROSAT* image can be attributed to absorption by these foreground clouds. In addition, several radiative optical emission features appear close to these obscuring dust regions, suggesting that G156 may be physically interacting with these clouds leading to the relatively bright radiative shock emission observed. It

should be noted, however, that the arc of patchy emission stretching from near the NE filament complex down toward the SW ridge of H α emission does not appear to be associated with dust features in the 6510 \AA optical continuum image, in the 60 μm *IRAS* image, or in the A_V extinction map, although it seemingly does run parallel to a stripe of fainter emission in the *ROSAT* X-ray image.

4 DISCUSSION

Our mosaic H α image of G156 (Fig. 1) shows a rather surprising amount of optical shock emission for a remnant previously reported to exhibit no detectable optical emission. G156's detected optical emission structure now ranks it among the most extensive seen among galactic remnants, albeit at the faint end of surface brightness. The lack of visibility of G156 on the Palomar Sky Survey is not particularly surprising given the broad passband of its images. Nor is it surprising that the SNR emission was not detected by Stecklum et al. (2004) who imaged a region around the Bok globule CB 26 close to the northwest filament complex in both H α and [S II], but were limited by a small (2') field of view. But the lack of detection by the narrow passband filter galactic plane survey of Parker et al. (1979) is puzzling. That survey's $l=155.5^\circ$, $b=+5^\circ$ plates are well centred on G156 and yet shows no discernible H α , [S II] $\lambda\lambda 6716, 6731$, or [O III] $\lambda 5007$ emission.

G156's detected optical emission consists of a considerable amount of both radiative and non-radiative filaments, something that is not commonly seen in SNRs. Only a handful of galactic remnants show such extensive non-radiative, Balmer-dominated emission filaments alongside considerable radiative filamentary nebulae. The few comparable objects include the Cygnus Loop, with its bright radiative west and east nebulae (NGC 6960 & 6995) and extensive Balmer-dominated filaments outlining much of the remnant's limb (Levenson et al. 1998), and RCW 86 with its lone but bright radiative emission SW limb region and non-radiative filaments outlining most of the rest of the remnant (Smith 1997).

The mixture of both radiative and non-radiative optical emission suggests that the remnant is situated in a highly non-homogenous ISM, with the radiative emission associated with relatively dense cloud–SNR interactions while the thin non-radiative filaments mark regions of much lower interstellar density. However, Pfeffermann et al. (1991) reported no spectral variations in four equally spaced sectors of the remnant, concluding that there was no significant variation in interstellar absorption across G156. They did find a range of N(H) column density of 9×10^{20} to $2 \times 10^{22} \text{ cm}^{-2}$ depending on the choice of model assumed, and chose the lower value in their final analysis. Yamauchi et al. (2000) estimated $N(\text{H}) = 3 - 4 \times 10^{21} \text{ cm}^{-2}$ using NEI plus thermal or power law models.

Neither study discussed the possibility of N(H) variations, and yet the presence of these large interstellar clouds along the line of sight clearly indicates that the foreground column density varies significantly across the face of the remnant. This complicates the assessment of the X-ray results, as the foreground density is position dependent on scales smaller than the effective apertures used in these studies. A

re-analysis of the *ROSAT* data is certainly warranted, using emission primarily from the relatively unobscured east side of the remnant.

The projected proximity and apparent alignment of the remnant's brighter radiative filaments with several foreground interstellar clouds and dust lanes hint at a possible physical interaction between the G156.2+5.7 remnant and these interstellar clouds. The estimated distance to the T-Tauri star V347 Aur associated with one of the southwestern foreground clouds is 250 – 300 pc (Cohen 1978), while the estimated distance to the Bok globule CB 26 near the remnant's bright northwest filament complex ranges from 140 to 300 pc (Launhardt & Henning 1977; Launhardt & Sargent 2001).

If G156 is indeed interacting with part of the Taurus–Auriga cloud complex in this direction, then the G156 remnant may be only ≈ 0.3 kpc distant, significantly closer than the previous X-ray derived estimates of 1.3 – 3 kpc. It would also be much younger than the 15,000 – 26,000 yr ages earlier analyses have suggested. In fact, assuming G156 is in the Sedov-Taylor (adiabatic) expansion phase of its evolution, lies at a distance of just 0.3 kpc, is expanding in an intercloud density of 0.2 cm^{-3} (Yamauchi et al. 1999, 2000), and was generated by a SN with energy around the canonical value of 1×10^{51} erg, then it has a radius of ≈ 5 pc, an age of ≈ 400 yr, and a shock velocity around 5000 km s^{-1} . Such a young age seems highly unlikely, as it should then have been seen as a historical supernova.

This extreme age problem is reduced somewhat if either the distance to the clouds is somewhat farther, or the ambient ISM density is higher. For example, at a distance of 0.6 kpc, a Sedov analysis of G156 would give an age of ≈ 2200 yr, and a shock velocity around 1500 km s^{-1} . Such an age would make G156 more akin to the SN 1006 SNR than the Cygnus Loop. Its nearly filled X-ray morphology is certainly unlike that seen in moderately old SNRs and an age of only a few thousand years would be more consistent with the observed presence of extensive non-radiative shock filaments which are most often seen associated with high-velocity shocks in young remnants. A relatively youthful remnant might also help explain the apparent enhanced abundances of Si and S seen in the X-ray spectra of the centre of G156 (Yamauchi et al. 1999).

On the other hand, the close apparent placement of the foreground clouds and the radiative emission could be simply a coincidence. Obviously, further investigations into the distance and general properties of this SNR are needed. For example, if its shock velocity is $\sim 1000 - 2000 \text{ km s}^{-1}$, then high resolution spectra of its Balmer dominated filaments should show evidence for a broad $H\alpha$ emission component like that seen in the filaments in Tycho and SN 1006. Moreover, these Balmer dominated filaments should exhibit large proper motions of order 1 arcsec yr^{-1} . Even null results would provide useful lower limits to the distance to G156, and hence lower limits on the age of the SNR. Whatever the outcome of future studies, G156 is clearly an interesting remnant, with a now recognized extensive and diverse optical emission structure.

ACKNOWLEDGMENTS

We thank J. Thorstensen for help with the optical coordinate matching. CLG is supported through UK PPARC grant PPA/G/S/2003/00040.

REFERENCES

- Blair, W. P., & Long, K. S. 1997, *ApJS*, 108, 261
 Busser, J.-U., Egger, R., & Aschenbach, B. 1996, *A&A*, 310, L1
 Claver, C. F. 1992, *BAAS*, 24, 1282
 Clemens, D. P., & Barvainis, R., 1988, *ApJS*, 68, 257
 Clemens, D. P., Yun, J. L., & Heyer, M. H., 1991, *ApJS*, 75, 877
 Cohen, M., 1978, *MNRAS*, 184, 695
 Cohen, M., 180, *AJ*, 85, 29
 Dobashi, K., Uehara, H., Kandori, R., Sakurai, T., Kaiden, M., Umemoto, T., Sata, F. 2005, *PASJ*, 57, 1
 Evans, I. N., & Dopita, M. A., 1985, *ApJS*, 58, 125
 Fesen, R. A., Blair, W. P., & Kirshner, R. P. 1985, *ApJ*, 292, 29
 Fesen, R. A., & Kirshner, R. P. 1980, *ApJ*, 242, 1023
 Finkbeiner, D. P. 2003, *ApJS*, 146, 407
 FitzGerald, M. P. 1968, *AJ*, 73, 983
 Green, D. A. 2004, *Bulletin of the Astronomical Society of India*, 32, 335 (<http://www.mrao.cam.ac.uk/surveys/snrs/>)
 Gull, T. R., Kirshner, R. P., & Parker, R. A. R. 1977, *ApJL*, 215, L69
 Kassim, N. E., Hertz, P., van Dyk, S. D., & Weiler, K. W. 1994, *ApJL*, 427, L95
 Kaplan, D. L., Gaensler, B. M., Kulkarni, S. R., & Slane, P. O. 2006, *ApJS*, 163, 344
 Launhardt, R., & Henning, Th., 1977, *A&A*, 326, 329
 Launhardt, R., & Sargent, A., 2001, *ApJ*, 562, L173
 Levenson, N. A., Graham, J. R., Keller, L. D., & Richter, M. J. 1998, *ApJS*, 118, 541
 Lorimer, D. R., Lyne, A. G., & Camilo, F. 1998, *A&A*, 331, 1002
 Lynds, B. T. 1962, *ApJS*, 7, 1
 Massey, P. & Gronwall, C. 1990, *ApJ*, 358, 344
 McGlynn, T., Scollick, K., White, N., *SkyView: The Multi-Wavelength Sky on the Internet*, McLean, B.J. et al., *New Horizons from Multi-Wavelength Sky Surveys*, Kluwer Academic Publishers, 1996, IAU Symposium No. 179, p465
 Neckel, Th., & Vehrenberg, H. 1985 “Atlas of Galactic Nebulae”, (Duesseldorf: Treugesell-Verlag), Vol. 1
 Osterloh, M., & Beckwith, S. V. W. 1995, *ApJ*, 439, 288
 Pannuti, T. G. & Allen, G. E. 2004, *Advances in Space Research*, 33, 434
 Parker, R. A. R. Gull, T. R. & Kirshner, R. P. 1979 “An Emission-Line Survey of the Milky Way”, NASA SP-434 (US Government Printing Office, Washington D.C.)
 Pfeffermann, E., Aschenbach, B., & Predehl, P. 1991, *A&A*, 246, L28
 Raymond, J. C. 1979, *ApJS*, 39, 1
 Rengelink, R. B., Tang, Y., de Bruyn, A. G., Miley, G. K., Bremer, M. N., Roettgering, H. J. A., & Bremer, M. A. R. 1997, *A&A*, 124, 259

- Reich, W., Fuerst, E., & Arnal, E. M. 1992, *A&A*, 256, 214
Reich, W., Berkhuijsen, E. M., & Sofue, Y. 1979, *A&A*, 72, 270
Seward, F. D., Dame, T. M., Fesen, R. A., & Aschenbach, B. 1995, *ApJ*, 449, 681
Smith, R. C. 1997, *AJ*, 114, 2664
Stecklum, B., Launhardt, R., Fischer, O., Henden, A., Leinert, C., & Meusinger, H. 2004, *ApJ*, 617, 418
Yamauchi, S., Koyama, K., Tomida, H., Yokogawa, J., & Tamura, K. 1999, *PASJ*, 51, 13
Yamauchi, S., Yokogawa, J., Tomida, H., Koyama, K., & Tamura, K. 2000, *Advances in Space Research*, 25, 567

This paper has been typeset from a \TeX / \LaTeX file prepared by the author.